The International Maritime Transport and Logistics (MARLOG 14) - ISSN 2974-3141
http://dx.doi.org/10.21622/MARLOG.2025.14.1.48
Artificial Intelligence Implementations Towards Shaping the Future of Digital World

LAYOUT OPTIMIZATION FOR OFFSHORE WIND FARMS CONSTRUCTION IN EGYPT: ACHIEVING MAXIMUM ENERGY EFFICIENCY

Abdallah M. Gobara (1), Elbadr O.Elgendi(2), Akram S. Elselmy (3) and Ahmed.S Shehta(4)

(1) Construction & Building Engineering, College of Engineering and Technology, Arab Academy for Science and Technology and Maritime Transport (AASTMT), Alexandria, Egypt, gobaraabdallah@gmail.com

(2) Construction & Building Engineering, College of Engineering and Technology, Arab Academy for Science and Technology and Maritime Transport (AASTMT), Alexandria, Egypt, elbadrosman@aast.edu

(3) Construction & Building Engineering, College of Engineering and Technology, Arab Academy for Science and Technology and Maritime Transport (AASTMT), Alexandria, Egypt, akram_soliman@aast.edu

(4) Marine and Offshore Engineering, College of Engineering and Technology, Arab Academy for Science and Technology and Maritime Transport, Alexandria, Egypt, a_samir@aast.edu.

ABSTRACT

Offshore wind farms are becoming increasingly widespread due to the vast ocean coverage and their potential for efficient energy generation in unobstructed areas. They represent a promising renewable energy source with minimal environmental impact, addressing global energy demands, climate change, energy supply challenges, and rising costs. A numerical study, employing a two-dimensional unsteady simulation, was conducted for an offshore wind farm along the Egyptian Mediterranean coast to determine the optimal spacing between turbines for maximum efficiency. The findings indicate that the enhanced model, with a layout of 4.8 rotor diameters along the x-axis and 3.2 rotor diameters along the y-axis, achieved an optimal configuration. This layout resulted in a performance increase of approximately 3% and a reduction in surface area occupancy by 16.3% compared to an existing offshore wind farm.

Keywords:

VAWTs flow interactions, Energy extractors' wake, Numerical optimization, Egyptian coasts, Renewable energy, Offshore farms.

1. INTRODUCTION

The pressing need to combat climate change, renewable energy has become vital in the shift toward a sustainable, low-carbon future. Offshore energy, in particular, offers substantial advantages by harnessing ocean and wind power to reduce reliance on fossil fuels. Recognizing the urgency, Egypt has emerged as an African leader in renewable energy, with a strong focus on wind power. Egypt has made substantial progress in renewable energy through large wind farms like those in the Gulf of Suez and Zaafarana, showcasing its commitment to sustainable energy. The 1000 Km span of the Mediterranean coast, in addition to ideal wind conditions, offers significant potential for expanding Egypt's efforts into offshore wind power, which supports Egypt's efforts to meet energy demands sustainably, advance regional climate goals, and strengthen energy independence through clean energy investments.

Offshore renewable energy is pivotal in the global transition to sustainable power, particularly through harnessing wind and wave resources for substantial energy production. Leading nations like the United

Kingdom and Denmark significantly reduce carbon emissions by relying on offshore wind (Yuhan et.al., 2022).[1] In Europe, the strategy aims to increase offshore wind capacity by 25 times by 2050 to meet carbon neutrality targets (Hasaballah, et. al.,2024).[3] The United States and China are also expanding offshore wind projects to enhance energy security and decrease fossil fuel dependence (Wang et al., 2022).[2] Thus, offshore renewable energy is crucial for diversifying energy portfolios and advancing global climate goals (Hasaballah, et. al.,2024).[3] The study aims at enhancing the layout for such a farm by specifying traverse and longitudinal spacing between farm turbines along Egypt's Mediterranean coast. Offshore wind farms face technical and economic challenges, notably wake effects, where closely spaced turbines experience reduced wind speed and increased turbulence due to interference from upwind turbines. This decreases energy output and heightens mechanical stress, impacting turbine performance and project feasibility. (Barthelmie & Jensen, 2010).[4]

Efficient construction site layouts optimization is vital for productivity, as poor planning can cause repeated handling and delays. Studies show that organized layouts reduce material handling costs by 20-60%. In the U.S., rework can add up to 30% to construction costs, labor operates at 40-60% efficiency, accidents account for 3-6% of expenses, and material waste is over 10%. Effective site planning is essential to reduce these inefficiencies and costs. (E. Mohamed, 2016). [5] Optimal spacing between turbines is essential to maximize efficiency and reduce the potential for accelerated wear and tear on the equipment. Additionally, wind farm layout influences the overall capital expenditure (CapEx) and operational expenditure (OpEx), as closer spacing might reduce initial setup costs but can lead to higher long-term maintenance costs due to the increased strain on the turbines (Myhr et al., 2014).[6]

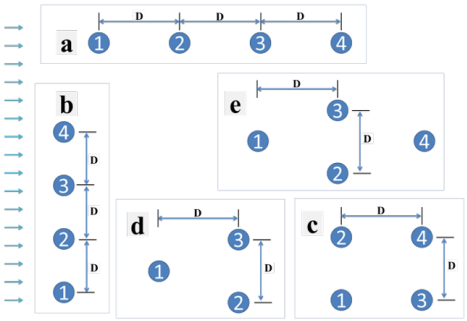

Figure 1: Different array configurations. (a & b) linear, (c) square, (d) triangle and (e) rhombus. (A.Ragab et.al 2020) [18]

Another significant consideration is operations and maintenance (O&M) costs, which are strongly correlated with the size and layout of the wind farm. Larger farms generally present higher O&M costs, given the challenges of maintaining remote and dispersed turbines in offshore environments, which often requires specialized vessels and technology (Carroll, *et.al,* 2016).[7] The distribution of turbines across a larger area can also impact both accessibility for maintenance crews and the frequency of required maintenance, as larger distances increase travel and downtime. Proper spacing can mitigate some of these costs by reducing interference and wear on individual turbines, thereby extending their operational lifespan and reducing the need for frequent maintenance (Jensen *et al.*, 2020).[8] Understanding and managing these constraints is critical to maximizing the economic and operational viability of offshore wind farms. Therefore, determining the optimal spacing not only affects energy production but also has long-term implications for the project's financial sustainability and alignment with environmental goals (Bak, Andersen, & Gaard, 2016). [9] From this perspective, reducing the farm-occupying surface area as much as possible without losing the output energy is a desired target.

Reaching this target requires optimizing the layout of the offshore wind farm. By using optimization techniques, planners can determine the exact location of each energy extraction unit within the farm's total area. A lot of array configurations are valid as shown in Figure 1. Optimal dimensions are achieved by defining the minimum and maximum separation distances (D) for an ideal layout. These distances allow energy extractors to be positioned for maximum energy capture across the farm without losses. This has been extensively studied using mathematical, numerical, and advanced optimization methods. (Chowdhury *et al*. 2010) [10] used the experimental data to optimize an array three by three wind turbine were spaced at distances of 3D and 7D along the y-axis and x-axis, respectively, utilizing the particle swarm optimization algorithm to maximize farm efficiency. The findings indicated that the power outputs were interdependent due to the wake effect.
Earlier research has outlined the key factors affecting energy farms, including the arrangement of the array, spacing between units, and the quantity of energy extractors. (A.Andres *et. al.* 2014) [11] An effective layout reduces the wake effect behind energy extractors. These factors have all been applied in the design of new offshore wind farms. Additionally, a crucial aspect is determining the spacing between energy extractors, supporting the concept of variable spacing currently used in existing offshore wind farms.

The typical spacing are ranging from 1.5D to 3D and 8D to 12D (M. R. Patel 1999) [12], 3D to 4D and 8D to 10D (S. Bhattacharya, 2017) [13], perpendicular to the prevailing wind and parallel to it in order. In addition, there are existing offshore wind farms, e.g. the Alpha Ventus which runs on a 6.5D, Horns Rev1 uses 7D (S. Astariz *et.al* 2015) [14], Bard using a 6D to 7.5D (D. W. GmbH, 2018) [15], and Lincs uses 6.25D to 10D (S. Astariz 2016) [16]. The latest optimizing trial ended up with 4D along y-axis and 5D along x-axis which revealed increasing in performance by 14.4% with 52.5% minimizing in the occupying surface area for the farm. (A.Ragab *et.al* 2021) [17]
The primary objective of this study is to enhance the existing offshore wind farm model by refining the turbine spacing, implementing incremental modifications of 0.2D rotor diameter (where D is the rotor diameter), as opposed to the 1D spacing used in previous research (A.Ragab *et.al* 2021) [17]. The study aligns with Egypt's strategic objective to expand the role of offshore renewable energy by optimizing the configuration and integration of offshore wind turbines (OWTs) within offshore energy farms. The aim is to determine the ideal separation distances (D) between energy extractors in both longitudinal and transverse directions, focusing on their impact on power coefficients. Given that data from the Egyptian offshore indicates wind speeds in the Mediterranean Sea range from 4.0 to 5.0 m/s, (G.Mosetti *et.al* 1994) [19] vertical axis wind turbines (VAWT) have been chosen for this analysis.

2. METHODOLOGY

The study employs a numerical analysis approach to design an energy farm by simulating various separation distances between turbines. The problem of optimizing offshore wind farm layout has various constraints, e.g. farm location, number of extractors, array layout, extractors' separating distance, and incident wind directions. An optimization framework is obtained through sequences of simulations.
These numerical simulations are divided into four phases, as illustrated in the flow chart, shown in Figure 2. In phase one, the numerical model is verified and validated. Next, in phase two, the model is investigated to extract the power coefficient. Then, in phase 3, modifying process to reach out the most optimum layouts and spacings. Finally, the farm layout and performances are examined in phase four. Using ANSYS Fluent software, the Unsteady Reynolds-Averaged Navier-Stokes (URANS) equations are solved to support the Sliding Mesh Motion (SMM) model, which simulates the rotation of turbine domains. The fluid domain is configured with dimensions of 80 meters by 50 meters along the x-axis and y-axis, respectively, establishing boundary conditions that accommodate the rotating turbine. The turbine is positioned 20 meters from the inlet and centered 25 meters between the two sides. After establishing this numerical model, simulations are conducted for multiple rotors arranged in three rows. The objective is to refine the model by decreasing the spacing between turbines by 0.2 D meters along both the x-axis and y-axis, aiming to enhance the optimal layout area based on recent

research findings which indicated that 4D, 5D along y-axis and x-axis respectively. (A.Ragab *et.al* 2021) [17].

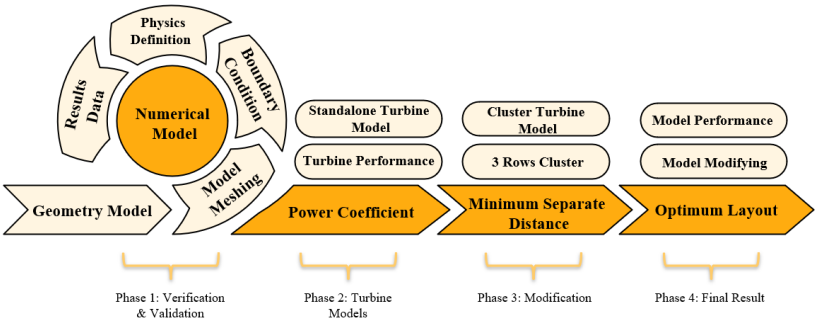

Figure 2: A schematic of the CFD simulations representing a road map of the obtained processes.

2.1. SOLUTION METHOD

All solver algorithms had tested, with negligible difference in the output aerodynamics coefficient same as observed before. (Gomez and Montlaur,2014) [21]. The sliding mesh motion (SMM) model is required for the rotating domains. It uses the Pressure-Based solver Coupled Solver algorithm (PBCS), as a spatial discretization method. However, it uses a double precision method for improving the analysis accuracy. As well as, using the unstructured mesh is required a solution model with the Least-Squares Cell-Based gradient interpolation methods.

Therefore, Pressure Interpolation scheme is used the Pressure Staggering Option (PRESTO) method to calculating the cell-face pressures, to overcome the high-speed flow rotation. Also, the momentum, turbulent kinetic energy, and turbulent dissipation rate methods are used the second order for Conservation Laws. The (Second Order) is a second order convection discretization scheme for unstructured meshes that allowing a higher accuracy in predicting the secondary flows, vortices, forces, etc. Also, Bounded Second Order Implicit model is selected for the transient formulation.

2.2. REFERENCE VALUES

A straight-bladed vertical axis wind turbine is selected for the present study. The blade transverse section is NACA 0021 type. (Castelli et al., 2011)[.20]. Boundary conditions include a uniform incident speed of 9.0 (m/s), with a wind direction heading from 0.0 (degree◦). The rotor torque coefficient (Cm) is calculated, as shown in equation (1):

$$C_m = \frac{M}{\frac{1}{2}\rho V^2 AL} \qquad (1)$$

Where M is the torque (N.m), ρ is the air density (Kg/m3), V is the air speed (m/s), A is the rotor swept area given by (A=D.H) in (m2), D is the overall rotor diameter (m), H is the rotor height (m), L is the reference length (m), and also v is the kinematics viscosity (m2/s). The power coefficient (CP) is computed in terms of the tip speed ratio (λ) and the rotor torque (M), as given by equation (2):

$$C_p = \frac{M\omega}{\frac{1}{2}\rho v^3 A} = C_m\lambda \qquad (2)$$

Where $\lambda=\omega R/V$, ω is the angular density (rad/s), and R is the rotor tip radius (m). In 2D simulations, the reference area (A) is taken as the turbine diameter (D), and the reference length (L) as the turbine radius. (Gomez and Montlaur,2014) [21]. The time-lapse is accounted for every 5.0◦ (degree◦) of the rotor rotation instead of 1.0◦ (degree) to cut down computational time. The corresponding minimum time step given by (Δt|5◦) is 0.002 (s), to achieve full 7.0 rotations, as shown in equation (3). (Gomez and Montlaur,2014) [21]

$$\Delta t|5^o = \frac{5}{\omega(rps).360} = \frac{5}{6.RPM} \qquad (3)$$

In the Fluent solver, the time step size (TSS) and the number of time step (NTS) can be set under menu Run Calculation. The equations can be written as follows in equation (4) and (5):

$$NTS = \frac{360}{\theta} \qquad (4)$$

$$TSS = \frac{N}{(\omega\ 0.15915) \times number\ of\ time\ step} \qquad (5)$$

Where N is the number of rotations (the value is determined by user), θ is the increment angle or time step rotation degree (the value is determined by user), ω is the turbine rotation speed (rad/s), 0.15915 is a constant to convert rad/s unit to rot/s unit. By trying 7 and 8 rotations to determine the suitable TSS, on one hand 7 rotations with NTS = 504 and on the other hand 8 rotations with NTS 576 it ended up with 7 rotations and time = 1.0067s so the result become stable and a moment coefficient selected as a final result is compared with experimental as illustrated in Figure 3.

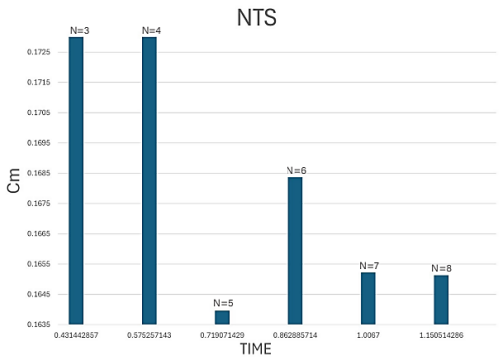

Figure 3: Shows the number of rotations where the solution become stable at N=7.

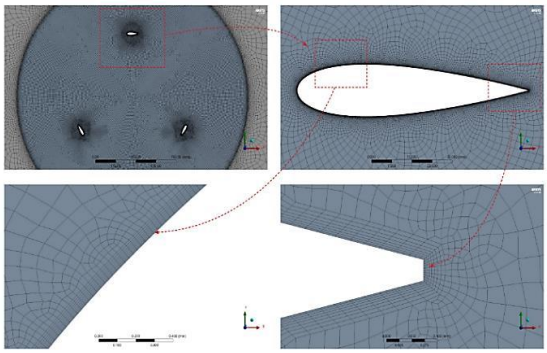

Figure 4: Turbine model with a close-up view of the hub meshing and domain interface illustration.

2.3. MESH INDEPDENCE

A high-resolution quadrilateral-dominant mesh is applied to both stationary and rotating domains using an automated method. The mesh covers the far field, hub, and control surface circles, with tailored refinements to ensure precise simulations and capture result gradients. Rotating zones, interacting with the three airfoil blades, require higher mesh density. Globally, the far field uses a coarse mesh with 0.0125 and 350 as minimum and maximum face sizes. A proximity and curvature sizing function is applied with fine settings and a curvature normal angle of 180.0. The control surface circles feature a fine 2.9 mm mesh, while the airfoil blade edges are divided into 10 segments Figure 4 and surrounded by 8 inflation layers with a first-layer height of 0.006 mm

Various simulations are conducted to assess mesh sensitivity and verify the model. The recommended initial mesh element counts falls between 300,000 and 600,000. Outcomes from each meshing scenario are compared with both the experimental data from (Castelli *et al.*, 2011).[20] and the numerical data from (Castelli *et al.*, 2011).[20], focusing on the moment coefficient along the airfoil blades and moment coefficient to confirm model accuracy. This is evaluated at a tip speed ratio (TSR) of (λ = 2.5) and a wind speed of 9.0 m/s, as used in the experiment (Castelli *et al.*, 2011).[20]. Based on the mesh independence study, a structured mesh comprising 380,355 elements was selected for the model. The study evaluated four mesh sizes: 348,486, 373,226, 380,355, and 591,307 elements, with corresponding moment coefficients (Cm) of 0.1537, 0.1652, 0.1669, and 0.1674, respectively. The results indicated that the difference in moment coefficients between the 380,355-element mesh and the 591,307-element mesh was less than 1% (approximately 0.3%). This minimal variation validates the adequacy of the 380,355-element mesh for achieving accurate and computationally efficient results, as shown in table 1.

Based on the latest research for (A.Ragab *et.al* 2021) [17] indicated that the most suitable turbulent model is Re-Normalized Group (RNG) k-epislon (k-ε) two equations' turbulence model with a Scalable Wall Function near wall treatment function is selected for its significantly accurate results over the other models tested throughout the simulations, and based on its properties. This model selection is based on (A.Ragab *et.al* 2021) [17] that was conducted between all the simulated turbulence models used for validation purposes, as shown in Figure 5 the Re-Normalized Group (RNG) k-epislon (k-ε) is validated with the experimental curve from (Castelli, *et al.*, 2010).[22]. the maximum TSR in the numerical study is identical with the experimental study. (TSR = 2.625)

Number of elements	*Cm*	*Status*
348,486	0.1537	Not Selected
373,226	0.1652	Not Selected
380,355	0.1669	Selected
591,307	0.1674	Not Selected

Table 1: Mesh Independence Study: convergence analysis of Cm with element counts

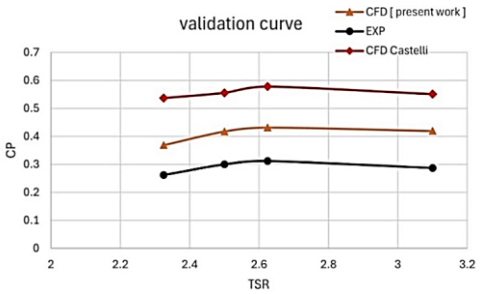

Figure 5: Average power coefficients (Cp) versus tip speed ratios (TSR) for turbulent models with different

3. RESULTS AND DISCUSSION

3.1. STANDALONE ROTOR

After validating the computational model with experimental data, separation distances (D) along both the x-axis and y-axis were systematically evaluated. A unidirectional wind speed of 4.5 m/s along the x-axis, representing typical conditions for the Egyptian North Coast, was applied for reference across various rotor configurations (G.Mosetti, et.al 1994) [19].The vertical axis wind turbine (VAWT) under examination is a three-bladed rotor with a NACA 0021 airfoil profile. This rotor, with a diameter of 1030 millimeters, rotates counterclockwise at an angular velocity of 43.68 rpm, as illustrated in Figure 6. The flow dynamics around an isolated rotor reveal a symmetric velocity profile along its longitudinal axis in the downstream direction, where axial velocity diminishes further downstream. The observed induced velocity ratio of 0.133 corresponds to a theoretical power coefficient (Cp) of 0.4, based on the ideal actuator disk theory. The computed Cp for this setup was found to be 0.42, closely aligning with the theoretical value. Notably, a minor increase in lateral velocity was detected at the rotor plane, potentially due to an additional small velocity component combined with blade tip vortex shedding effects. The local flow field surrounding each of the three rotor blades varies significantly due to the distinct flow incidence at each rotational position. In certain angular positions, the flow may separate when the incidence exceeds the stall angle, which is visibly illustrated in Figure 7 across three angular positions.

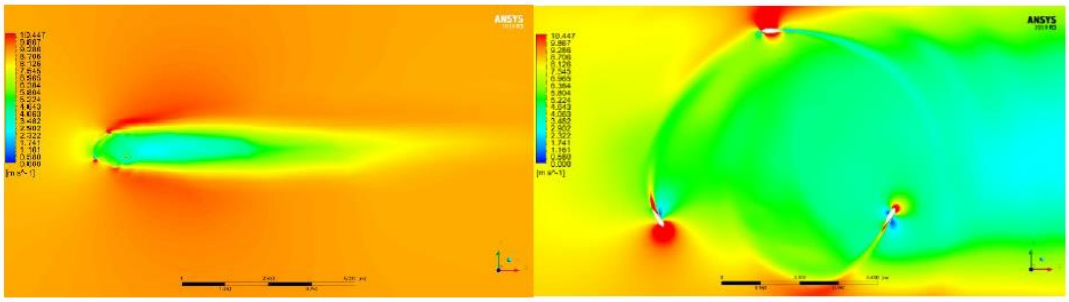

Figure 6: Velocity field past a single VAWT rotor.

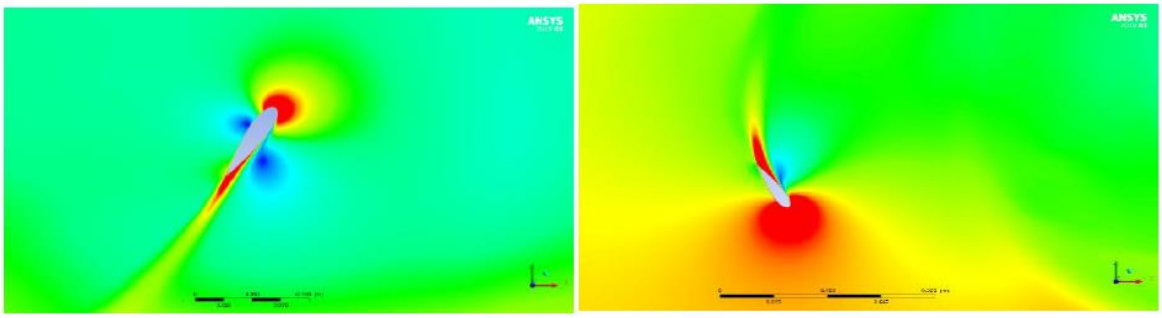

Figure 7: A close-up view for the local flow velocity field around blades.

3.2. MULTIPLE ROTORS

The proposed staggered layout with specific spacing is applied to a farm-scale configuration, with three rotor rows arranged in a square staggered array as shown in Figure 8. This layout was used to study flow interactions between rotor wakes on a smaller scale. The staggered arrangement provided performance advantages by optimizing flow dynamics. Among the configurations tested, the 4D x 5D spacing along the x- and y-axis yielded the best performance (A.Ragab et.al 2021) [19]. Table 2 provides a comprehensive comparison of various wind array layouts in terms of their average power coefficient (Cp), overall performance relative to a reference layout, and area reduction. The reference layout, set at 5D spacing along the x-axis and 4D along the y-axis, serves as a baseline for assessing the impact of different spacing configurations on energy performance and spatial efficiency.

The results as shown in the illustrative graph Figure 9 that decreasing the spacing along either the x or y-axis generally leads to reduced overall performance, as indicated by negative values in the "Overall Performance" column. For example, a layout with 4.6D x-spacing and 4D y-spacing experiences a performance drops of -3.845%, one of the most significant decreases observed. This reduction suggests that closer rotor spacing increases wake interactions, which can diminish efficiency. Therefore, reducing rotor spacing should be approached cautiously to avoid compromising energy output.

Array layout X,Y directions	*Average (Cp)*	*Overall Performance*	*Area Reduction*
5D,4D (Reference)[**18**]	-	-	-
4.8D,4D	0.415	-1.274%	4%
4.6D,4D	0.404	-3.845%	8%
4.8D,3.8D	0.416	-1.141%	8.8%
5D,3.8D	0.414	-1.517%	5%
4.8D,3.6D	0.415	-1.201%	13.6%
4.8D,3.4D	0.422	0.429%	15%
4.8D,3.2D	0.432	2.892%	23.2%
4.8D,3D	0.413	-1.797%	28%

Table 2: Overall offshore wind array layout Performance

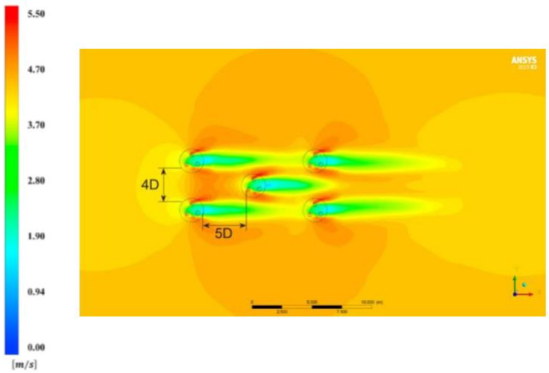

Figure 8: Three rows of five VAWT rotors.

The data also reveal a notable impact on spatial efficiency. Configurations with greater reductions in y-axis spacing tend to achieve significant area savings. For instance, the layout with 4.8D spacing along the x-axis and 3.2D along the y-axis achieves a substantial area reduction of 23.2%, while also showing an overall performance increase of 2.892%. This configuration demonstrates the potential

for balancing performance enhancements with spatial efficiency, making it particularly advantageous for high-density offshore wind farms where space is limited.

Among the configurations tested, the 4.8D x-spacing and 3.2D y-spacing layout emerges as an optimal choice, showing the highest increase in overall performance (2.892%) along with considerable area reduction (23.2%). This layout suggests a well-balanced configuration where both energy efficiency and spatial footprint are optimized, making it potentially suitable for maximizing output within limited areas in offshore wind farm installations.

Conversely, some layouts achieve considerable area reductions but at a noticeable performance cost. For instance, the layout with 4.8D x-spacing and 3D y-spacing yields the largest area reduction (28%) but results in a performance decline of -1.797%. This indicates that while aggressive reductions in spacing are possible, they may lead to inefficiencies in power generation due to increased wake interference. Therefore, a balance must be struck between minimizing surface area and maintaining adequate performance levels. To wrap up, the table highlights that optimizing turbine spacing can enhance the efficiency of offshore wind arrays by balancing power generation with spatial compactness. The configuration with 4.8D x-spacing and 3.2D y-spacing stands out as the most favorable, offering an effective trade-off between performance and area reduction as illustrated in Figure 10. These findings underscore the importance of strategic layout design in achieving both operational efficiency and spatial economy in offshore wind farm developments.

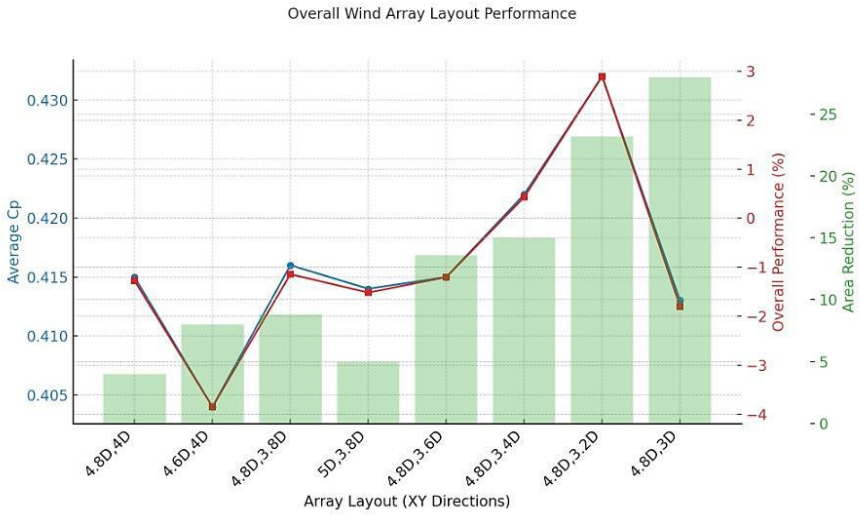

Figure 9: The graph illustrates the effect of minimizing the spacing between rotors and its reflection on power coefficient and occupied area.

3.3. ECONOMIC ASSESSMENT

Optimizing offshore wind farm layouts has a direct impact on both capital expenditures (CAPEX) and operational expenditures (OPEX). A compact layout reduces installation costs by decreasing cabling and potentially reducing the number of substations, as seen in denser configurations like the 4.8D x 3.2D layout, that reduce occupation by up to 23.2% which can lower costs associated with infrastructure according to (Peng *et al.*, 2019).[23] However, closer turbine spacing can also increase wake effects and turbulence, affecting structural integrity and potentially raising CAPEX due to the need for stronger foundations (Mishnaevsky, 2021)[24]. Therefore, it is essential to balance reduced spacing for CAPEX and OPEX savings with spacing that minimizes wake interference and maximizes energy efficiency.

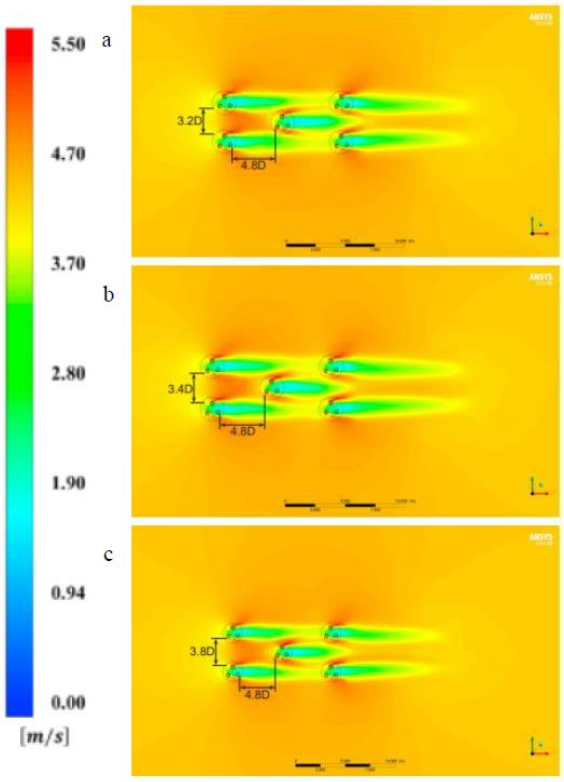

Figure 10: Three rows of five VAWT rotors with incident wind of 4.5 m/ s (TSR = 2.625)/The rotors separated by fixed 3.2D with 3.4D, 3.8D, and 4.8 D along x-axis and y-axis in (a), (b), and (c) respectively.

4. CONCLUSION

This study enhances offshore wind farm designs by refining turbine spacing in 0.2D increments to improve power efficiency and optimize spatial utilization. This research aligns with Egypt's strategic objective to advance offshore wind energy systems. Turbine interactions were analyzed using ANSYS Fluent, employing advanced simulation techniques such as the Unsteady Reynolds-Averaged Navier-Stokes (URANS) equations and the Sliding Mesh Motion (SMM) model. The findings underscore the significance of layout optimization in offshore wind farm design, enabling a reduction in land usage while maintaining or enhancing power output, a crucial aspect of sustainable energy development. The results demonstrate that strategic adjustments in turbine spacing have a significant impact on both area reduction and aerodynamic performance. Among the configurations tested, the layout with reduced spacing of 4.8D (longitudinal) and 3.2D (transverse) achieved a notable 23.2% reduction in occupied area while increasing the power coefficient (Cp) by 2.892%, indicating substantial potential for improving efficiency in dense wind farm setups. Additionally, configurations such as 4.6D (longitudinal) and 3.6D (transverse) offered a balanced approach, achieving a 13.6% area reduction with only a minor decrease in overall performance (-1.201%).

5. FUTURE WORK

Future work will focus on employing genetic algorithms to optimize the turbine spacing further. This approach will enable the exploration of a vast range of layout possibilities, ensuring the identification of the most efficient configuration for offshore wind farms. By leveraging genetic algorithms, the optimization process will become more robust and capable of addressing the complexities associated with large-scale wind farm designs.

6. REFERENCES

1) Yuhan Chen, Heyun Lin, (2022). Overview of the development of offshore wind power generation in China. Sustainable Energy Technologies and Assessments, https://doi.org/10.1016/j.seta.2022.102766

2) Ye, X., Wang, H., & Ma, S. (2023). Estimation of soil organic carbon stocks using a machine learning approach with remote sensing data in the Loess Plateau, China. *Environmental Development*, 45, 100814. https://doi.org/10.1016/j.envdev.2022.100814

3) Hasaballah, A. H., Khairy, A., & El-Aziz, M. A. (2024). Investigating the Impacts of Climate Change on Coastal Environments Using Remote Sensing and GIS Techniques. *Environments*, 11(9), 199. https://doi.org/10.3390/environments11090199

4) Barthelmie, R. J., & Jensen, L. E. (2010). Evaluation of wind farm efficiency and wind turbine wake effects in offshore wind farms. *Wind Energy*, 13(6), 573–586. https://doi.org/10.1002/we.408

5) E. Mohamed Mohamed Osman Ahmed Elgendi Thesis, (2016) "An automated dynamic site layout planning system-a case study of egypt,"

6) Myhr, A., Bjerkseter, C., Ågotnes, A., & Nygaard, T. A. (2014). Levelised cost of energy for offshore floating wind turbines in a life cycle perspective. *Renewable Energy*, 66, 714-728. https://doi.org/10.1016/j.renene.2014.01.017

7) Carroll, J., McDonald, A., & McMillan, D. (2016). Failure rate, repair time and unscheduled O&M cost analysis of offshore wind turbines. *Wind Energy*, 19(6), 1107-1119. https://doi.org/10.1002/we.1887

8) Jensen, K., Liew, R., & Patterson, D. (2020). Optimization of offshore wind farm layout using cost function analysis. *Energy*, 187, 115993. https://doi.org/10.1016/j.energy.2019.115993

9) Bak, C., Andersen, P. B., & Gaard, J. (2016). Cost-effective strategies for offshore wind farm layout optimization considering wake effects. *Journal of Physics: Conference Series*, 753, 082002. https://doi.org/10.1088/1742-6596/753/8/082002

10) S. Chowdhury, A. Messac, J. Zhang, L. Castillo, and J. Lebron,(2010) "Optimizing the unrestricted placement of turbines of differing rotor diameters in a wind farm for maximum power generation," in International Design Engineering Technical Conferences & Computers and Information in Engineering Conference, Montreal, Quebec, Canada,: ASME https://doi.org/10.1115/DETC2010-29129

11) A. D. d. Andrés, R. Guanche, L. Meneses, C. Vidal, and I. Losada, (2014) "Factors that influence array layout on wave energy farms," Ocean Engineering, Elsevier Journal, vol. 82, pp. 32–41,. https://doi.org/10.1016/j.oceaneng.2014.02.027

12) M. R. Patel, (1999) "Wind and solar power systems," PHD, CCR press, Taylor & Francis. https://doi.org/10.1201/9781003042952,

13) S. Bhattacharya,(2017) "Civil engineering aspects of a wind farm and wind turbine structures," Guildford, United Kingdom: Wind Energy Engineering, Elsevier Inc. , 2017 pp. 221-242. 10.1109/ICPEA49807.2020.9280096

14) S. Astariz, J. Abanades, C. Perez-Collazo, and G. Iglesias, (2015) "Improving wind farm accessibility for operation & maintenance through a co-located wave farm: Influence of layout and wave climate," Energy Conversion and Management, vol. 95, no. 0, pp. 229-241, https://doi.org/10.1016/j.enconman.2015.02.040

15) D. W. GmbH, "Status of offshore wind energy development in Germany," ed, (2018).
16) S. Astariz, C. Perez-Collazo, J. Abanades, and G. Iglesias, (2016)"Hybrid wave and offshore wind farms: A comparative case study of co-located layouts" International Journal of Marine Energy vo..15, pp.2-16https://doi.org/10.3390/en17051240
17) Ragab, A. M., Shehata, A. S., Elbatran, A. H., & Kotb, M. A. (2021). *Numerical optimization of hybrid wind-wave farm layout located on Egyptian North Coasts*. *Ocean Engineering*, 234, 109260. https://doi.org/10.1016/j.oceaneng.2021.109260
18) Ragab, A.M., Shehata, A.S., Elbatran, A.H., Kotb, M.A., (2020). Preliminary design of an offshore wind farm on the Egyptian coast. International Conference on Power and Energy Applications. IEEE Xplore: Busan, South Korea, pp. 159-163. 10.1109/ICPEA49807.2020.9280096
19) G. Mosetti, C. Poloni, and B. Diviacco,(1994) "Optimization of wind turbine positioning in large wind farms by means of a genetic algorithm," Wind Engineering and Industrial Aerodynamics, vol. 51, pp. 105-116,. https://doi.org/10.20508/ijrer.v13i2.13839.g8746
20) Castelli, M.R., Englaro, A., Benini, E.. (2011) The Darrieus wind turbine: proposal for a new performance prediction model based on CFD. Energy 36 (8), 4919-4934. https://doi.org/10.1016/j.energy.2011.05.036
21) Gomez, A.H., Montlaur, A.d.V.d..(2014) "Computational Fluid Dynamics Study of 2D Vertical axis Turbines for Application to Wind and Tidal Energy Production. BSc". http://hdl.handle.net/2099.1/24458
22) M. R. Castelli, G. Ardizzon, and L. Battisti,(2010) "Modeling strategy and numerical validation for a darrieus vertical axis micro-wind turbine," in *ASME, International Mechanical Engineering Congress & Exposition IMECE2010*, Vancouver, British Columbia, Canada, https://doi.org/10.1115/IMECE2010-39548
23) Peng Hou, Jiangsheng Zhu (2019). A review of offshore wind farm layout optimization and electrical system design methods. *Journal of Modern Power System and Clean Energy DOI: 10.1007/s40565-019-0550-5*
24) Mishnaevsky, L. (2022). Root causes and mechanisms of failure of offshore wind turbines: A review. *Renewable and Sustainable Energy Reviews*, 148, 111309. https://doi.org/10.3390/ma15092959